Report on a problem studied at the UK Mathematics-in-Medicine Study Group Loughborough 2008
< http://www.maths-in-medicine.org/uk/2008/bioreactors/ >

Multiscale modelling of bioreactors for growing bone tissue

Ian Hewitt (University of Oxford),
Igor Chernyavsky (University of Nottingham),
Alistair Middleton (University of Nottingham),
John Fozard (University of Nottingham),
Clare Bailey (University of Loughborough),
Colin Please (University of Southampton),
John King (University of Nottingham),
Ian Halliday (Sheffield Hallam University),
John Ward (University of Loughborough),
Chris Breward (University of Oxford).

Problem presented by
Diganta Das (University of Loughborough) and
Norazharuddin Abdullah (University of Oxford).

Report prepared by
Clare Bailey (University of Loughborough),
Igor Chernyavsky (University of Nottingham),
John Fozard (University of Nottingham),
Ian Hewitt (University of Oxford),
Alistair Middleton (University of Nottingham).

November 28, 2008

1 Introduction

A large number of bone-grafting procedures are performed annually to repair diseased bones and bone loss caused by fractures and cancers. Whilst surgeons prefer to use autografts (the patient's own bone), these may be limited in availability and can result in donor-site morbidity (damage at the site from which the graft is removed). Allografts (bone from cadavers) are also limited in availability, incorporate less well into existing bone, and may have impaired structural strength [1–4]. There is therefore interest in alternative materials for skeletal repair; these need to have appropriate structural properties, and it is desirable that they also encourage the formation of new bone and the regeneration of the patient's original tissue. One possibility is to culture suitable cells (e.g. mesenchymal stem cells) within the scaffold; when implanted, these may

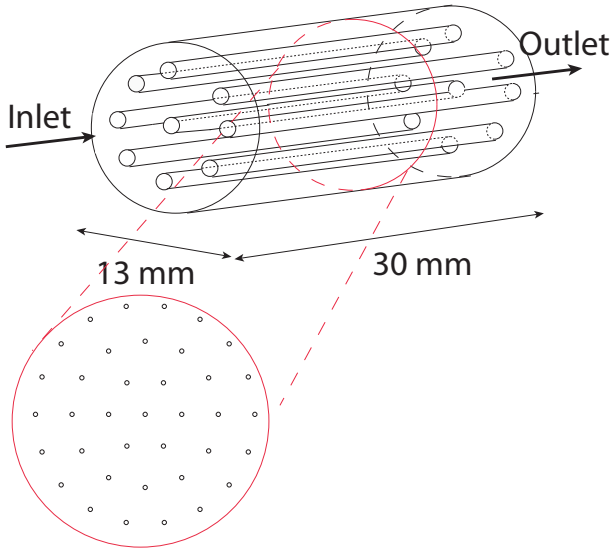

Figure 1: Schematic diagram of a hollow fibre membrane bioreactor. The hollow fibres (narrow cylinders) can be seen to run through the scaffold (wide cylinder); note that the small number of fibres depicted here are merely representative of the large number (~ 200) in the current design. Nutrient medium is made to flow down the lumens of the fibres, this fluid being supplied at the inlet and removed at the outlet.

differentiate into bone-forming cells (osteoblasts) and may also generate extracellular matrix components and diffusible signalling molecules that recruit the patient's own cells to colonise the scaffold and generate bone tissue.

Cell growth within a tissue-engineering scaffold is limited by the supply of nutrients and oxygen, and the removal of waste products. The dominant transport mechanism in a scaffold is diffusion, and cells in a tissue mass supplied by this route are only viable within ~ 100 μm of sources of oxygen and glucose. Implants for skeletal repair need to be thicker than this, so hollow fibre membrane bioreactors (HFMBs) have been developed to overcome this restriction. These consist of a scaffold in which many small, semi-permeable hollow fibres are embedded, mimicking the capillary networks found tissues such as bone. Culture medium containing nutrients is made to flow through the fibres, so nutrients and waste products need only diffuse the small distance from/to the nearest fibre, rather than to the outside of the implant.

The aim of this study-group problem is to investigate the transport and kinetics of nutrients within HFMBs. The problem presenters wish to increase the scale of the bioreactor and are keen to understand which combinations of quantities (dimensionless groups) affect the nutrient transport problem.

2 Hollow fibre membrane bioreactors

The current design of the HFMB is shown in Figure 1. Cells are distributed (initially relatively uniformly) in a scaffolding material; at present, this is an agarose gel that allows the diffusion of oxygen, nutrients and waste products

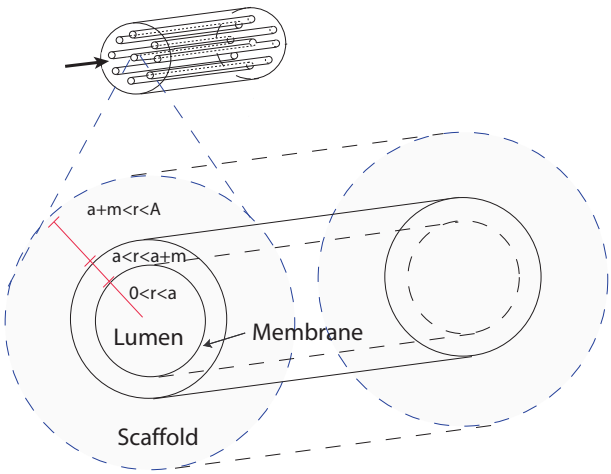

Figure 2: Geometry of the Krogh cylinder. Each cylinder contains a hollow fibre, with $0 < r < a$ being the lumen and $a < r < a + m$ the membrane, and an annular region $a + m < r < A$ of scaffolding material (agarose gel) in which cells are present.

but does not permit a bulk flow of fluid. Approximately 200 hollow fibres (HFs) run through the scaffold. These are hollow tubes with an internal diameter of 200 μm, and are constructed from a 20 μm thick membrane which permits the diffusion of substances of up to 10 kDa in molecular weight. The HFs are approximately parallel and equally spaced in the HFMB, and run between two end plates. The HFs and scaffold are contained within a sealed module, with inlets and outlets through which nutrient medium is pumped. This fluid flows along the lumens of the HFs, and nutrients such as glucose and oxygen diffuse out through the membranes and into the scaffold. Conversely, waste products diffuse into the lumens of the HFs and are removed through advection.

The cells are cultured in this system for approximately one month. The total cell number drops rapidly near the start of the experiment (possibly due to damage sustained during the fabrication of the scaffold), but subsequently increases to approximately 20% more than its starting value. In order for the cells to be viable in the HFMB, it is important that local nutrient levels lie within an appropriate range. It is also desirable that the final implant contains a roughly uniform distribution of cells; depending on the sensitivity of cell kinetics to nutrient concentrations this may further limit acceptable variations in nutrient concentration levels.

We now examine nutrient transport within the HFMB. The intent of this calculation is to quantify how the nutrient concentration in the scaffold (in particular, its spatial variations) depends on the parameters of the problem. Whilst there will be an initial transient period (during which the nutrient diffuses into those regions furthest from the HFs), the timescale of this ($O(A^2/D_s) \sim$

$1 - 10$ min, see Table 1) is much shorter than both the duration of the experiments (28 days) and the time-scale on which the cell density may vary (a typical cell-cycle duration being 1 day). As a consequence we will consider the nutrient concentration to be at a steady-state.

Ideally, the fibres in the HFMB would be exactly parallel and uniformly spaced, but limitations of the manufacturing process mean that there is always some variation in their positions. Whilst it would be possible to solve the transport problem numerically in the precise geometry (reconstructed from sections of the HFMB, or using tomography), this would be computationally expensive and give limited physical insight.

Instead, we will adopt the Krogh cylinder approximation [5] (see the review [6, 7]); this assumes that the HFMB is composed of numerous identical cylindrical regions (one of which is shown in Figure 2) with impenetrable outer boundaries. We further assume that the nutrient concentrations in each cylinder are axisymmetric, depending only on the distance from the mid-line of the cylinder, r, and the axial distance, z. The Krogh cylinder or "tissue cylinder" approximation is valid in the case of isotropic passive diffusion of solutes in the scaffold and describes a representative average unit of the metabolic exchange [8, 9].

While the radius of a representative Krogh cylinder has been measured experimentally ($A \simeq 0.32$ mm, see Table 1), we can obtain an estimate using the given number of fibres ($N = 200$) and the outer diameter of the bioreactor ($2R_0 = 13$ mm) [10]. A rough area-based estimate is $\pi R_0^2 = N\pi A^2$, in which case

$$A = \frac{R_0}{\sqrt{N}} \simeq 0.5 \text{ mm}.$$

We can also estimate of the Krogh cylinder radius from the the experimental protocol used to form a hexagonal array. We start from a single fibre in the centre and place six equispaced fibres at the fixed distance d. Then we add 12 new fibres on a concentric circle of radius $2d$, etc. until we fill the whole bioreactor (see Fig. 3). From the geometrical design of the array, we can see

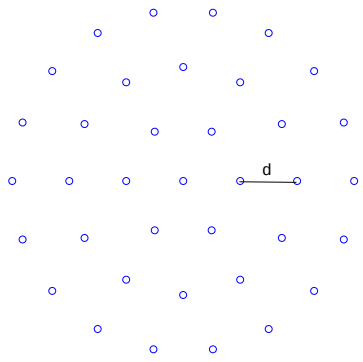

Figure 3: An approximation of the hexagonal array of fibres in the HFMB.

that the number of fibres on each circle constitutes an arithmetical progression with $a_1 = 6$, $a_p = 6p$, where p is the number of concentric circles. Therefore, the

total number of the fibres is $N = 1 + 6p(p+1)/2$ so $2p \simeq -1 + \sqrt{(4N-1)/3}$. Since the outer radius $R_0 = p\,d$ and the distance between the centres of two adjacent fibres $d = 2A$, we estimate the Krogh cylinder radius to be

$$A = \frac{R_0}{\sqrt{(4N-1)/3} - 1} \simeq 0.4 \text{ mm}\,.$$

For both these estimates, the radius of the Krogh cylinder decreases as $1/\sqrt{N}$ for large N, and so halving the radius requires four times as many fibres.

2.1 Formulation

In this section we consider the concentration, c, of a substance which may be either glucose or oxygen; whilst the uptake rates and diffusion coefficients of these two substances differ, the transport problem takes the same form in either case. Within the lumen of the HFs ($0 < r < a$) the nutrient diffuses with diffusion coefficient D_l and is advected by the flow. At the relatively low Reynolds numbers under consideration here ($\mathrm{Re} = Ua/\nu \simeq 0.75$, see Tables 1 and 2), the entry length is a small fraction of the tube diameter; as the aspect ratio of the fibres is small we will assume that the flow within the lumen is fully developed Poiseuille flow (the axial velocity, u, being $u = 2U_0(1-r^2)$). Note that, as we believe the permeability of the membrane (in the porous medium sense) to be very small, we impose no-slip conditions on the flow at the lumen-membrane boundary (rather than those of Beavers and Joseph [11]).

In the membrane ($a < r < a + m$) and the scaffold ($a + m < r < A$), the sole transport mechanism is diffusion, with diffusion coefficients D_m and D_s in each medium, respectively. At each interface between media we require continuity of the concentration, c, and the normal diffusive flux, $-D\partial c/\partial r$, and on the outer boundary of the Krogh cylinder we require that the normal flux vanishes. We assume that there is a constant number density of cells, n, throughout the scaffold, and that the nutrient uptake rate of each cell is either proportional to the concentration of nutrients (first-order kinetics, with constant of proportionality k_1) or constant (zeroth-order kinetics, with k_0 being the uptake rate). Note that if the uptake rates for the two choices of kinetics are to agree at a concentration C, then $k_0 = Ck_1$.

For first-order cell kinetics, the dimensional form of the nutrient transport problem (assuming no dependence on the azimuthal variable) is

$$2U_0(1-r^2)\frac{\partial c}{\partial z} = D_l\left(\frac{1}{r}\frac{\partial}{\partial r}\left(r\frac{\partial c}{\partial r}\right) + \frac{\partial^2 c}{\partial z^2}\right), \quad 0 < r < a, \tag{1a}$$

$$D_m\left(\frac{1}{r}\frac{\partial}{\partial r}\left(r\frac{\partial c}{\partial r}\right) + \frac{\partial^2 c}{\partial z^2}\right) = 0, \qquad a < r < a + m, \tag{1b}$$

$$D_s\left(\frac{1}{r}\frac{\partial}{\partial r}\left(r\frac{\partial c}{\partial r}\right) + \frac{\partial^2 c}{\partial z^2}\right) = k_1 nc, \qquad a + m < r < A, \tag{1c}$$

in $0 < z < L$. The boundary conditions on this advection-diffusion problem are that the nutrient concentration at the inlet of the lumen is C_0, and that the boundaries between the membrane or scaffold and the outside of the Krogh

cylinder are impermeable. In order for this problem to be mathematically well-formulated, we need to also impose suitable boundary conditions (zero axial derivative) on the nutrient concentration at the outlet of the lumen. Along with continuity of concentrations and diffusive fluxes at interfaces between media, these conditions become

$$
\begin{aligned}
&\text{on } z=0,\ 0<r<a, && c = C_0,\\
&\text{on } z=0,\ a<r<A, && \frac{\partial c}{\partial z} = 0,\\
&\text{on } z=l,\ 0<r<A, && \frac{\partial c}{\partial z} = 0,\\
&\text{at } r=0, && \frac{\partial c}{\partial r} = 0,\\
&\text{at } r=a, && D_l \left.\frac{\partial c}{\partial r}\right|_{a-} = D_m \left.\frac{\partial c}{\partial r}\right|_{a+}, \qquad c|_{a-} = c|_{a+},\\
&\text{at } r=a+m, && D_m \left.\frac{\partial c}{\partial r}\right|_{(a+m)-} = D_s \left.\frac{\partial c}{\partial r}\right|_{(a+m)+}, \quad c|_{(a+m)-} = c|_{(a+m)+},\\
&\text{at } r=A, && \frac{\partial c}{\partial r} = 0.
\end{aligned}
$$

Here $c\big|_{a-}$ denotes the limiting value of the concentration as we approach the lumen-membrane boundary ($r = a$) from the lumen ($r < a$), whilst $c\big|_{a+}$ denotes the limit as we approach the boundary from the membrane ($r > a$), and similarly for the other interfaces. For zeroth-order kinetics, equation (1) in the scaffold is replaced by

$$
D_s \left(\frac{1}{r}\frac{\partial}{\partial r}\left(r\frac{\partial c}{\partial r}\right) + \frac{\partial^2 c}{\partial z^2}\right) = k_0 n, \qquad a+m<r<A.
$$

Estimates of the dimensional parameters for the current design of the HFMB are listed in Table 1.

2.2 Non-dimensionalisation

We rescale the variables of the problem according to

$$
u = U_0 \hat{u}, \qquad c = C_0 \hat{c}, \qquad r = a\hat{r}, \qquad z = l\hat{z},
$$

where U_0 is the average axial flow velocity along the lumens. On dropping hats, the problem in the Krogh cylinder becomes

$$
\mathrm{Pe}(1-r^2)\frac{\partial c}{\partial z} = \frac{1}{r}\frac{\partial}{\partial r}\left(r\frac{\partial c}{\partial r}\right) + \epsilon^2 \frac{\partial^2 c}{\partial z^2}, \qquad 0<r<1, \tag{2a}
$$

$$
\frac{1}{r}\frac{\partial}{\partial r}\left(r\frac{\partial c}{\partial r}\right) + \epsilon^2 \frac{\partial^2 c}{\partial z^2} = 0, \qquad 1<r<1+\delta, \tag{2b}
$$

$$
\frac{1}{r}\frac{\partial}{\partial r}\left(r\frac{\partial c}{\partial r}\right) + \epsilon^2 \frac{\partial^2 c}{\partial z^2} = \mathrm{Da}\, c, \qquad 1+\delta<r<R, \tag{2c}
$$

Parameter	Value	Reference
Fibre inner radius (a)	1.0×10^{-4} m	[12]
Fibre membrane thickness (m)	2.0×10^{-5} m	[12]
Krogh cylinder radius (A)	3.2×10^{-4} m	[12]
Fibre length (l)	3.0×10^{-2} m	[12]
Average axial flow velocity (U_0)	0.745×10^{-2} m/s	[12]
Fluid kinematic viscosity (ν)	$\sim 10^{-6}$ m^2/s	
Diffusivity of glucose in the lumen ($D_l^{(\mathrm{g})}$)	0.54×10^{-9} m^2/s	[10, 12]
Diffusivity of oxygen in the lumen ($D_l^{(\mathrm{o})}$)	3.0×10^{-9} m^2/s	[10, 12]
Diffusivity of glucose in the membrane ($D_m^{(\mathrm{g})}$)	0.54×10^{-10} m^2/s	[10, 12]
Diffusivity of oxygen in the membrane ($D_m^{(\mathrm{o})}$)	3.0×10^{-10} m^2/s	[10, 12]
Diffusivity of glucose in the scaffold ($D_s^{(\mathrm{g})}$)	1.08×10^{-10} m^2/s	[10, 12]
Diffusivity of oxygen in the scaffold ($D_s^{(\mathrm{o})}$)	6.0×10^{-9} m^2/s	[10, 12]
Inlet concentration of glucose ($C_0^{(\mathrm{g})}$)	5.55 mol/m^3	[12]
Inlet concentration of oxygen ($C_0^{(\mathrm{o})}$)	0.22 mol/m^3	[12]
Cell seeding density (n)	2.0×10^{12} cells/m^3	[12]
Glucose uptake rate per cell ($k_0^{(\mathrm{g})}$)	3.83×10^{-16} mol cell^{-1} s^{-1}	[12]
Oxygen uptake rate per cell ($k_0^{(\mathrm{o})}$)	3.75×10^{-17} mol cell^{-1} s^{-1}	[12]
Glucose consumption rate coefficient ($n\,k_1^{(\mathrm{g})} = n\,k_0^{(\mathrm{g})}/C_0^{(\mathrm{g})}$)	1.38×10^{-4} s^{-1}	
Oxygen consumption rate coefficient ($n\,k_1^{(\mathrm{o})} = n\,k_0^{(\mathrm{o})}/C_0^{(\mathrm{o})}$)	3.41×10^{-4} s^{-1}	
Glucose degradation rate in the water/acidic environment	$\sim 10^{-5} - 10^{-4}$ s^{-1}	[13]

Table 1: Dimensional parameter values used in the model.

with boundary and continuity conditions

$$\text{at } z = 0,\ 0 < r < 1, \qquad c = 1, \tag{3a}$$

$$\text{on } z = 0,\ 1 < r < R, \qquad \frac{\partial c}{\partial z} = 0, \tag{3b}$$

$$\text{on } z = 1,\ 0 < r < R, \qquad \frac{\partial c}{\partial z} = 0, \tag{3c}$$

$$\text{at } r = 0, \qquad \frac{\partial c}{\partial r} = 0, \tag{3d}$$

$$\text{at } r = 1, \qquad \left.\frac{\partial c}{\partial r}\right|_{1-} = D_m^* \left.\frac{\partial c}{\partial r}\right|_{1+}, \qquad c|_{1-} = c|_{1+}, \tag{3e}$$

$$\text{at } r = 1+\delta, \quad D_m^* \left.\frac{\partial c}{\partial r}\right|_{(1+\delta)-} = D_s^* \left.\frac{\partial c}{\partial r}\right|_{(1+\delta)+}, \quad c|_{(1+\delta)-} = c|_{(1+\delta)+}, \tag{3f}$$

$$\text{at } r = R, \qquad \frac{\partial c}{\partial r} = 0. \tag{3g}$$

The dimensionless parameters are the aspect ratio of the fibre lumen, ϵ, the dimensionless membrane thickness, δ, the normalised diffusion coefficients, D_m^* and D_s^*, the dimensionless Krogh cylinder radius R, the (reduced) Péclet number, Pe, and the Damköhler number, Da, defined by

$$\epsilon = \frac{a}{l}, \quad \delta = \frac{m}{a}, \quad D_m^* = \frac{D_m}{D_l}, \quad D_s^* = \frac{D_s}{D_l}, \quad R = \frac{A}{a},$$
$$\mathrm{Pe} = \frac{2U_0 l}{D_l}\frac{a^2}{l^2}, \quad \mathrm{Da} = \frac{k_1 n a^2}{D_s}.$$

The Péclet number relates advection of nutrient along the lumen to diffusion across its radius, whilst the Damköhler number relates the uptake rate of nutrients to the time taken for them to diffuse (radially) across the scaffold. For zeroth-order kinetics we have

$$\frac{1}{r}\frac{\partial}{\partial r}\left(r\frac{\partial c}{\partial r}\right) + \epsilon^2\frac{\partial^2 c}{\partial z^2} = \mathrm{Da}_0, \qquad 1+\delta < r < A, \tag{4}$$

instead of (2c), where the Damköhler number is now taken to be

$$\mathrm{Da}_0 = \frac{k_0 n a^2}{D_s C_0}.$$

Estimates of the dimensionless parameters, based on the data of Table 1, are presented in Table 2. For the current choice of dimensional parameters Da can be seen to be very small, in which case we expect uptake by the cells to have a minimal effect on the concentration of nutrients in the bioreactor (we will see in §2.6 that $R^2\mathrm{Da}$ is the important combination of dimensionless parameters). However, Da can be increased by increasing the cell seeding density, n, or the nutrient uptake rate, k_1, and it is conceivable that these could be somewhat larger in practice than the current estimates. Alternatively, if the estimates for the cell density and uptake rate are roughly correct, the HFs are perhaps

unnecessarily closely spaced; the (overall) diameter of the bioreactor could be increased, or the number of fibres decreased (until $R^2\mathrm{Da}$ is no longer small). In the numerical solutions considered later (Figures 5–10), we will consider larger values for Da (Da = 0.1, 0.3 or 1).

Parameter	Symbol	Value
Fibre (lumen) aspect ratio	ϵ	3×10^{-3}
Dimensionless membrane thickness	δ	0.2
Dimensionless Krogh cylinder radius	R	3.2
Normalised diffusivity in the membrane	D_m^*	0.1
Normalised diffusivity in the scaffold	D_s^*	0.2
Péclet number for glucose	$\mathrm{Pe}^{(\mathrm{g})}$	9.2
Péclet number for oxygen	$\mathrm{Pe}^{(\mathrm{o})}$	1.7
Damköhler number for glucose	$\mathrm{Da}^{(\mathrm{g})}$	1.3×10^{-2}
Damköhler number for oxygen	$\mathrm{Da}^{(\mathrm{o})}$	0.57×10^{-2}
Reynolds number (based on lumen diameter)	Re	0.75

Table 2: Non-dimensional parameter values.

The aspect ratio ϵ is small, and in the subsequent analysis we will neglect all terms of $O(\epsilon)$ or smaller, which is equivalent to ignoring diffusive transport in the axial direction. (We also ignore the boundary conditions (3b) and (3c), which will generate boundary layers of thickness $O(\epsilon)$ near $z = 0$ and $z = 1$.) As the Péclet number, Pe, is large and the Damköhler number, Da, small, it would be consistent to also neglect terms of $O(\mathrm{Da})$ and $O(1/\mathrm{Pe})$; however, this would give us that the concentration everywhere is to leading-order the same as that at the inlet. We wish to quantify the variations in the nutrient concentrations, and so retain these terms. Note that, for any practical HFMB, Da will be at most $O(1)$ in size (and is likely to be small), otherwise the nutrient concentration will decay significantly away from the fibres and cells will not be viable except in small regions near them.

2.3 First-order kinetics

We now consider the solution of (2) for first-order cell kinetics. The solution within the membrane ($1 < r < 1 + \delta$) is

$$c = c\big|_{1-} + \frac{1}{D_m^*}\frac{\partial c}{\partial r}\bigg|_{1-} \log r, \tag{5}$$

using (3e), continuity of concentration and flux at the lumen-membrane boundary $r = 1$. On applying the conditions (3f) at the membrane-scaffold interface ($r = 1 + \delta$), we obtain jump conditions relating the concentration and fluxes at the inner boundary of the scaffold with those at the outer boundary of the lumen, namely

$$c\big|_{1+\delta+} = c\big|_{1-} + \frac{\log(1+\delta)}{D_m^*}\frac{\partial c}{\partial r}\bigg|_{1-}, \tag{6}$$

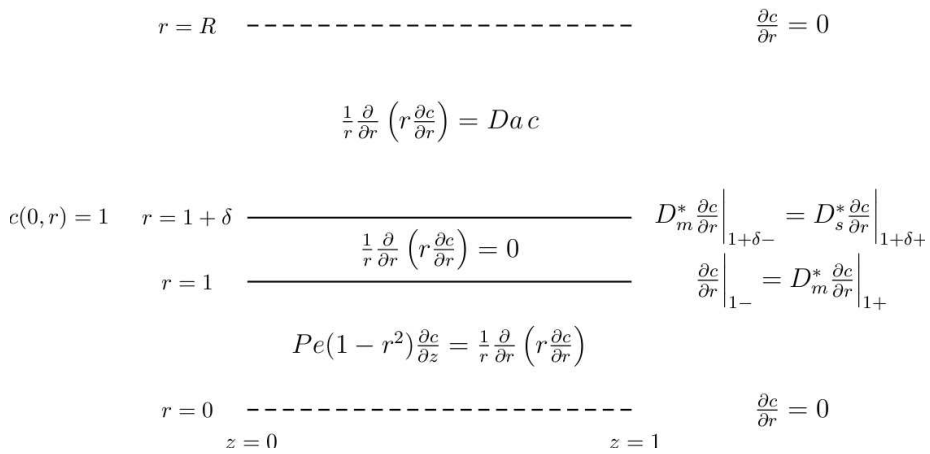

Figure 4: Krogh cylinder problem (in dimensionless variables) in the small aspect ratio ($\epsilon \ll 1$) limit. The outer radius $r = R$ is indicative of the spacing between fibres (relative to the diameter of the fibres). The conditions shown on the right are that the normal diffusive flux is continuous at interfaces between media; c itself is continuous throughout the cylinder.

$$\left.\frac{\partial c}{\partial r}\right|_{1+\delta+} = \frac{1}{D_s^*}\frac{1}{1+\delta}\left.\frac{\partial c}{\partial r}\right|_{1-}. \tag{7}$$

The solution to (2c) is a linear combination of the modified Bessel functions $K_0(r\mathrm{Da}^{1/2})$ and $I_0(r\mathrm{Da}^{1/2})$. The condition (3g) at $r = R$ requires the gradient be zero there, and on imposing (6) we find that

$$c = \left(c\big|_{1-} + \frac{\log(1+\delta)}{D_m^*}\left.\frac{\partial c}{\partial r}\right|_{1-}\right) \times \left(\frac{K_0(rDa^{1/2})I_0'(R\mathrm{Da}^{1/2}) - K_0'(R\mathrm{Da}^{1/2})I_0(rDa^{1/2})}{K_0((1+\delta)\mathrm{Da}^{1/2})I_0'(R\mathrm{Da}^{1/2}) - K_0'(R\mathrm{Da}^{1/2})I_0((1+\delta)\mathrm{Da}^{1/2})}\right) \tag{8}$$

within the scaffold ($1 + \delta < r < R$). Applying (7) then gives

$$\left(1 - \frac{\log(1+\delta)}{D_m^*}D_s^*(1+\delta)\mathrm{Da}^{1/2}\kappa\right)\left.\frac{\partial c}{\partial r}\right|_{1-} = D_s^*(1+\delta)\mathrm{Da}^{1/2}\kappa c\big|_{1-}, \tag{9}$$

a Robin boundary condition upon the nutrient concentration in the lumen ($0 < r < 1$), where

$$\kappa = \frac{K_0'((1+\delta)\mathrm{Da}^{1/2})I_0'(R\mathrm{Da}^{1/2}) - K_0'(R\mathrm{Da}^{1/2})I_0'((1+\delta)\mathrm{Da}^{1/2})}{K_0((1+\delta)\mathrm{Da}^{1/2})I_0'(R\mathrm{Da}^{1/2}) - K_0'(R\mathrm{Da}^{1/2})I_0((1+\delta)\mathrm{Da}^{1/2})}. \tag{10}$$

Once the solution has been found in the lumen, the solution elsewhere is given by (5) for $1 < r < 1+\delta$ and (8) for $1+\delta < r < R$. (Note that this simplification is only valid when the cell density in the scaffold is uniform.)

The problem in the lumen is

$$Pe(1-r^2)\frac{\partial c}{\partial z} = \frac{1}{r}\frac{\partial}{\partial r}\left(r\frac{\partial c}{\partial r}\right), \tag{11}$$

with boundary conditions

$$c = 1 \qquad \text{at} \quad z = 0, \tag{12a}$$

$$\frac{\partial c}{\partial r} = 0 \qquad \text{at} \quad r = 0, \tag{12b}$$

$$\frac{\partial c}{\partial r} = -\lambda c \qquad \text{at} \quad r = 1, \tag{12c}$$

where the constant λ is given (with κ from (10)) by

$$\lambda = \frac{D_s^* D_m^* (1+\delta)\mathrm{Da}^{1/2}\kappa}{\log(1+\delta) D_s^* (1+\delta)\mathrm{Da}^{1/2}\kappa - D_m^*}. \tag{13}$$

We solve (11)–(13) numerically by first replacing derivatives with respect to r by central differences in space, and then solving the resulting system of ordinary differential equations in z using the MATLAB routine `ode15s`. These numerical solutions are shown in Figure 5 for a number of different choices for the dimensionless parameters, where we also plot the solutions (5) and (8) in the membrane and the scaffold. Figure 6 shows the radial profiles of the solutions at the outlet end of the bioreactor ($z = 1$), where the concentrations are smallest; this clearly shows the dependence on the parameters Pe (i.e. the speed at which nutrients are pumped through) and Da (i.e. the rate at which they are consumed by the cells).

It is worth simplifying the problem in the limit where $R^2\mathrm{Da}$ and δ are both small (the former condition being that the radius of the Krogh cylinder is small relative to the length-scale on which the nutrient concentration decays, $\mathrm{Da}^{-1/2}$). In this case,

$$\kappa \sim -\frac{(R^2-1)\mathrm{Da}^{1/2}}{2}$$

and

$$\lambda \sim \frac{D_s^* \mathrm{Da}}{2}(R^2-1).$$

Here $\mathrm{Da}(R^2-1)/2$ is the total nutrient uptake rate of the cells in the annular scaffold region (per unit azimuthal angle), so the boundary condition (12c) is easily understood as a requirement that the flux out of the lumen be equal to the cross-sectionally integrated consumption rate in the scaffold. The ratio D_s^* appears because of the different diffusion coefficients within lumen and scaffold. By expanding the Bessel functions for small argument, the solution (8) in the scaffold can be written as

$$c(z,r) \sim c(z)\big|_{1-}\left[1 - \frac{\delta}{D_m^*}\frac{D_s^*\mathrm{Da}}{2}(R^2-1) - \frac{R^2\mathrm{Da}}{2}\log r\right]. \tag{14}$$

We retain the term containing δ/D_m^* because the normalised diffusion coefficient in the membrane, D_m^*, may be of comparable size to δ. This term supplies the jump in concentration between the outer boundary of the lumen and the inner boundary of the scaffold, which is clearly apparent in the solutions of Figure 6.

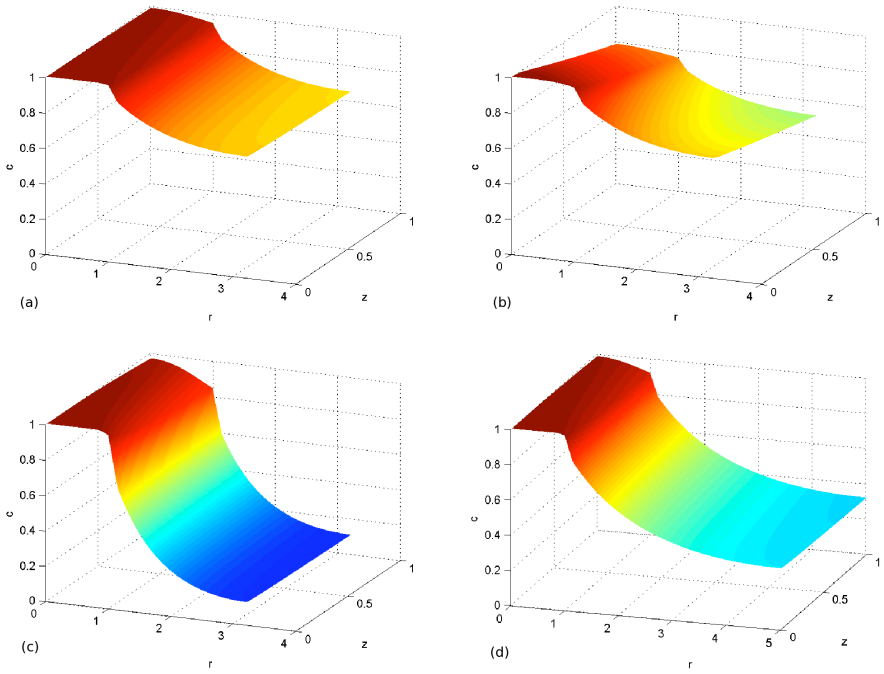

Figure 5: Nutrient concentration, c, in the Krogh cylinder, obtained from numerical solution of the problem (11)–(12) in the fibre lumen and from (5) and (8) in the membrane and scaffold, respectively. The variables are all dimensionless: the radial variable, r, scaled with the radius of the lumen, the axial distance, z, scaled with the the length of the bioreactor and the nutrient concentration, c, scaled with that at the inlet. Discontinuities in the concentration gradient can be observed at the lumen-membrane ($r = 1$) and membrane-scaffold ($r = 1 + \delta$) boundaries. The outer (Krogh) radius is $R = 3.2$. (a) Here Pe $= 10$ and Da $= 0.1$, as may be roughly appropriate for the current bioreactor. (b) As in (a), but with reduced Péclet number Pe $= 1$, Da $= 0.1$. (c) As in (a), but with increased Damköhler number Pe $= 10$, Da $= 1$. (d) As in (a) (Pe $= 10$, Da $= 0.1$), but with the outer radius at $R = 5$, corresponding (for a lumen radius of 100 μm) to a Krogh cylinder radius of 500 μm. The colours indicate the same nutrient concentration in all plots.

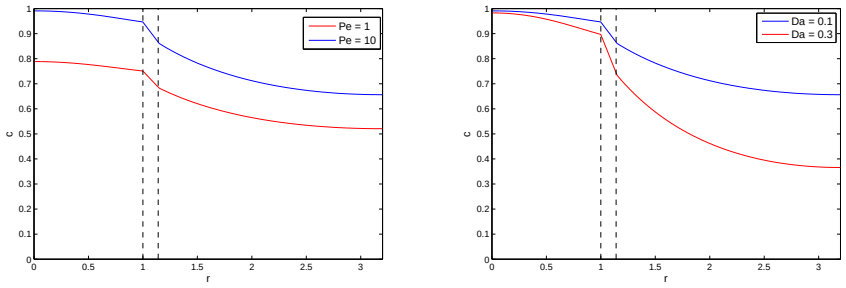

Figure 6: Concentration of nutrient c at $z = 1$ (outlet end of bioreactor) from numerical solutions of (11)–(12) in the lumen, and (5) or (8) elsewhere. The left-hand plot shows solutions with $\mathrm{Da} = 0.1$ and $\mathrm{Pe} = 1$ or $\mathrm{Pe} = 10$, and the right-hand plot shows solutions with $\mathrm{Pe} = 10$ and $\mathrm{Da} = 0.1$ or $\mathrm{Da} = 0.3$. Vertical dashed lines indicate the position of the membrane.

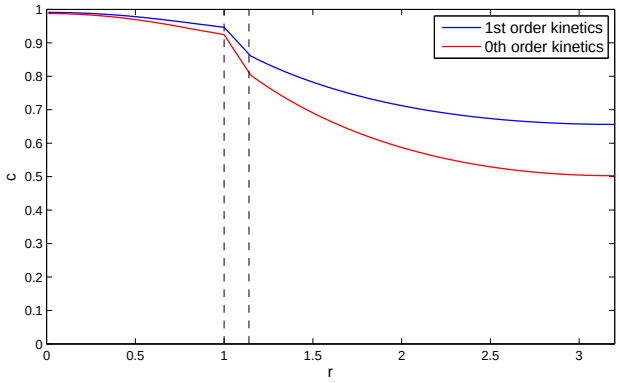

Figure 7: Comparison of solutions at $z = 1$ for first order kinetics (reaction rate linear in concentration) and zeroth-order kinetics (reaction rate constant). As in Figure 6, with the Péclet number $\mathrm{Pe} = 10$ and the Damköhler number 0.1 in each case ($\mathrm{Da} = 0.1$ or $\mathrm{Da}_0 = 0.1$).

2.4 Zeroth-order kinetics

For zeroth-order kinetics, the solution of (4) in the scaffold is

$$c = \frac{\mathrm{Da}_0}{2}\left[\frac{r^2-(1+\delta)^2}{2} - R^2\left(\log r - \log(1+\delta)\right) - \frac{\log(1+\delta)}{D_m^*} D_s^*\left(R^2-(1+\delta)^2\right)\right] + c\Big|_{1-}, \tag{15}$$

and the solute concentration in the fibre membrane is

$$c = -\frac{D_s^*}{D_m^*}\frac{\mathrm{Da}_0}{2}\left[R^2-(1+\delta)^2\right]\log r + c\Big|_{1-}. \tag{16}$$

The boundary condition (12) for the system (11)–(12) now becomes

$$\left.\frac{\partial c}{\partial r}\right|_{1-} = -\lambda_0\,, \tag{17}$$

where

$$\lambda_0 = D_s^*\frac{\mathrm{Da}_0}{2}\left[R^2-(1+\delta)^2\right].$$

Again, the problem in the lumen must be solved numerically, and once this is done the solutions in the scaffold and membrane are given by (15) and (16), respectively.

A comparison of the solutions for first- and zeroth-order kinetics is shown in Figure 7, where we see that more nutrient is consumed in the zeroth order case. This is expected since the consumption rate does not decrease as the amount of nutrient decreases as in the first-order case.

2.5 Analytical approximation

In Figure 5, the concentration appears to be relatively uniform in the cross section of the cylinder. If we *assume* that c in the lumen is independent of r, then integrating over its cross section gives

$$\begin{aligned}\frac{\mathrm{Pe}}{4}\frac{\partial c}{\partial z} &= \left.\frac{\partial c}{\partial r}\right|_{1-} - \left.\frac{\partial c}{\partial r}\right|_{0+}\\ &= -\lambda c,\end{aligned}$$

where the boundary contributions come from (12b)–(12c), λ being defined in (13). The solution to this is

$$c = e^{-4\lambda z/\mathrm{Pe}}, \tag{18}$$

giving the approximate solution in the fibre lumen, and from (5) and (8), the approximate solutions in the other regions are

$$c(z,r) = e^{-4\lambda z/\mathrm{Pe}}\left(1 - \frac{\lambda}{D_m^*}\log r\right) \tag{19}$$

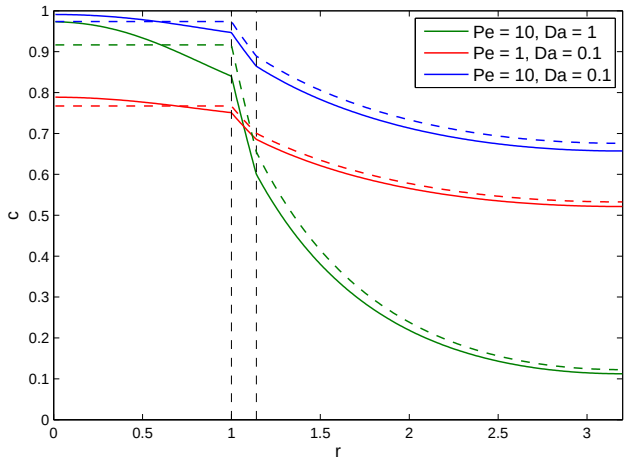

Figure 8: Comparison of numerical solutions of the Krogh cylinder problem ((11)–(12) in the lumen, and (5) or (8) elsewhere) and the approximate analytical solutions (18)–(20), at the outlet end of the HFMB ($z = 1$) for different values of the Péclet number, Pe, and the Damköhler number, Da. The smallest concentration, occurring at $r = R$, appears to be reasonably well approximated.

in the membrane ($1 < r < 1 + \delta$) and

$$c(z,r) = e^{-4\lambda z/\mathrm{Pe}} \left(1 - \frac{\lambda}{D_m^*}\log(1+\delta)\right) \times \frac{K_0(r\mathrm{Da}^{1/2})I_0'(R\mathrm{Da}^{1/2}) - K_0'(R\mathrm{Da}^{1/2})I_0(r\mathrm{Da}^{1/2})}{K_0((1+\delta)\mathrm{Da}^{1/2})I_0'(R\mathrm{Da}^{1/2}) - K_0'(R\mathrm{Da}^{1/2})I_0((1+\delta)\mathrm{Da}^{1/2})}, \quad (20)$$

in the scaffold ($1 + \delta < r < R$). This approximation is compared with the numerical solution of the (small aspect ratio) Krogh cylinder problem ((11)–(12) in the lumen, and (5) or (8) elsewhere) in Figure 8, where the radial profiles are compared at the outlet end of the bioreactor ($z = 1$). The approximation gives an acceptable prediction of the minimum concentration at $r = R$ and the profile in the scaffold. The approximation works particularly well if Pe is either large or small, because in these cases the profile in the lumen is close to being flat.

2.6 Concentration variations

We are interested in quantifying the variations in concentration within the bioreactor, and are therefore particularly interested in the minimum value, which will occur at the point furthest from the inlet and the fibre, namely $z = 1, r = R$ (see Figure 5). It is evident from (2) that this minimum concentration can depend only on the 6 dimensionless parameters R, Pe, Da, D_m^*, D_s^* and δ. When δ is small it is only important in combination with D_m^*; δ/D_m^* gives the jump in c across the membrane. We will assume for the purposes of discussion that D_s^* and D_m^* (the ratios of diffusion coefficients in membrane and scaffold to that in the lumen) are fixed, along with the thickness of the membrane, δ. We can

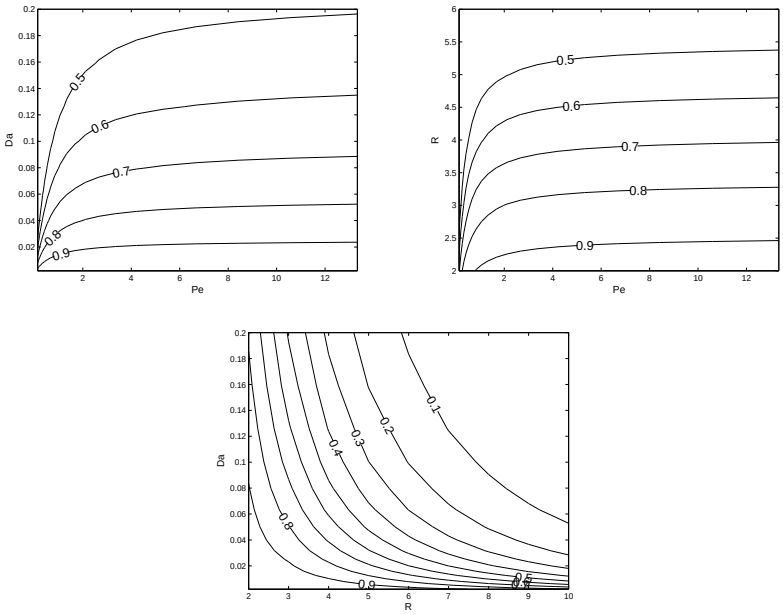

Figure 9: Minimum values of the nutrient concentration (relative to $c = 1$ at the inlet), which occurs at $z = 1$, $r = R$. These values are calculated from the numerical solution of the (small aspect ratio) Krogh cylinder problem. In each plot, two out of the three parameters R, Pe and Da are varied and the other fixed (at $R = 3$, Da $= 0.04$ or Pe $= 10$).

then consider how the solutions depend on the remaining three parameters R, Da and Pe. Physically this corresponds to varying the spacing of fibres, the nutrient uptake rate or the density of cells, and the length of the bioreactor or the nutrient flow speed. Figure 9 shows how the minimum value of c (again, obtained from the numerical solution of the Krogh cylinder problem) varies as a function each pair of these parameters while holding the other one fixed. If an allowable tolerance for the concentration variations is decided on, it is easy to read off the appropriate range of dimensionless parameters which can then be converted to the physical parameters of the experiment.

However, in the limit in which R^2Da is small, the solutions depend on R and Da only through this combination (this is evident from the asymptotic forms for λ (14) and c in the scaffold (14)). This limit is of practical importance, as it corresponds to situations where the radial decay in concentration is small. In Figure 10, we plot the minimum value of c as a function of the two parameters Pe and R^2Da.

3 Conclusions and further work

In this report, we examined nutrient transport in a HFMB using the Krogh cylinder approximation to simplify the geometry of the problem. Seven dimensionless parameters governing nutrient transport were identified in §2.2 (see Table 2; note that the flow in the lumens will be Poiseuille provided that the

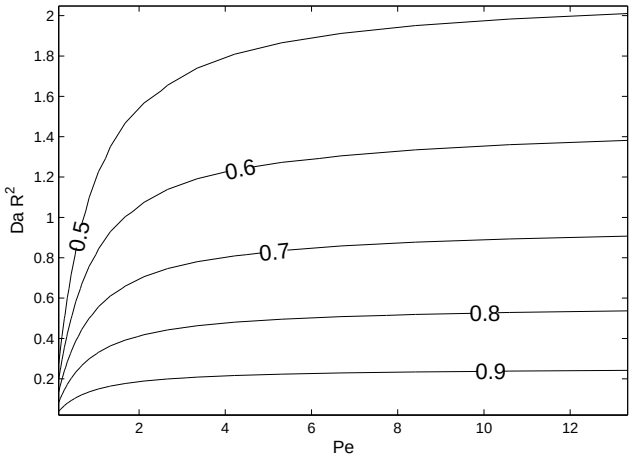

Figure 10: Minimum values of the nutrient concentration ($c = 1$ at inlet), which occur at $z = 1$, $r = R$, in terms of the two dimensionless numbers R^2Da and Pe on which the solutions depend for small R^2Da. If the allowable variation in concentration is between 70–100% of the inlet concentration, for instance, the values of the dimensionless parameters should be kept below the 0.7 curve, by designing the physical parameters of the bioreactor appropriately. It should be noted that the solutions start to depend independently on R and Da when R^2Da is no longer small, and Figure 9 should then be referred to.

Reynolds number is not large, so this parameter does not affect the transport problem). For the current design, the aspect ratio of the fibres, ϵ, (and that of the Krogh cylinder, ϵR) is small, so we simplified the problem by ignoring axial diffusion. Further assuming the solution in the Krogh cylinder to be axisymmetric, we reduced the three-dimensional transport problem in multiple materials to a two-dimensional problem in the fibre lumen that was straightforward to solve numerically (§§2.3–2.4). We also examined (§2.5) the (somewhat heuristic) approximation in which the concentration within the lumen is assumed to be uniform in each cross section. We obtained analytical expressions for the concentration, and confirmed numerically (Figure 8) that these gave reasonable approximations to the concentration variations in the scaffold of the HFMB.

Assuming that the cross-sectional geometry of the hollow fibres and the material properties of the membrane and scaffold could not be readily modified left us with three dimensionless parameters, R, Pe and Da, which could be varied by changing the fibre spacing, bioreactor length, flow rate in the fibres and cell density. In §2.6, we examined numerically how these three parameters affected the variation in nutrient concentration in the HFMB. In the limit where radial variation was small ($R^2\text{Da} \ll 1$), the minimum concentration was found to depend on just two combinations of these parameters; therefore, if only small variations are acceptable, it is relatively simple to determine the appropriate range of physical parameters for the bioreactor design from Figure 10.

The presented analysis is equally applicable to the evacuation of cells' waste products (e.g. CO_2 and lactic acid) from the scaffold. It seems reasonable to assume zeroth-order kinetics for waste production c_w: $D_s \nabla^2 c_w = -k_p(c)\, n$,

where the production rate k_p may depend on the nutrient concentration c. For constant production rate, the concentration profiles would be the inverse of those shown in Figure 7, with the maximum concentration being at the outer edge of the Krogh cylinder.

The current model predicts nutrient variations in the HFMB for a given uniform distribution of cells. In practice, the local number density of cells will vary over the course of the experiment. Cell kinetics (death and division rates) may depend on the local concentrations of nutrients and waste products, in which case the distribution of cells will become non-uniform, and this process could be self-reinforcing in some circumstances. In order to include such effects, the cell number density, n, needs to be treated as a dependent variable of the system; we expect that it will be governed by an equation of the form

$$\frac{\partial n}{\partial t} = \mu \nabla^2 n + R(c, n),$$

where μ is the random motility of the cells (which may be small in practice) and the kinetic term, $R(c, n)$, includes the effects of cell proliferation and death. The form of R and its sensitivity to changes in cell density and nutrient concentrations are important, and it is likely that further experiments (cell proliferation assays) would be necessary to determine these.

Whilst the current scaffolding material is not observed to degrade over the course of the experiments, this may be significant for future versions of the design, and it is also possible that the cells may generate extracellular matrix proteins; both of these processes could affect the diffusion coefficient in the scaffold. However, unless the cell density becomes very large, we expect that nutrient transport through cells will only have a small effect on the bulk diffusion coefficient of the scaffold (the relative change being proportional to the volume fraction occupied by the cells [14]).

In conclusion, we have identified nutrient diffusion in the scaffold as the main limitation in transporting nutrients to cells; the further apart the fibres are placed the more variable the nutrient concentration within the scaffold will be. For the current operating regime, our model predicts that variations in concentration within each cross section will be much greater than those along the axis of the bioreactor. Whilst the maximum variation is expected to be small, this may become more substantial if the cell density is increased.

We have established a suitable model with which to predict variations in nutrient concentration and it is relatively straightforward to extend this to account for changes in cell density over time. To understand the effect of concentration variations on the distribution of cells in the HFMB, more data is required on the sensitivity of cell kinetics to nutrient concentrations. Through examining the time-dependent behaviour of the cell density (coupled to the nutrient concentration), and requiring the density at the end of the culture to be sufficiently uniform (for the implant to be useful medically), it may be possible to estimate practical bounds on allowable nutrient concentration variations.

References

[1] C G Finkemeier. Bone-grafting and bone-graft substitutes. *J. Bone Joint Surg. Am.*, 84(3):454–464, March 2002.

[2] A S Greenwald, S D Boden, V M Goldberg, Y Khan, C T Laurencin, and R N Rosier. Bone-graft substitutes: Facts, fictions, and applications. *J. Bone Joint Surg. Am.*, 83:S98–103, November 2001.

[3] C F Lord, M C Gebhardt, W W Tomford, and H J Mankin. Infection in bone allografts. Incidence, nature, and treatment. *J. Bone Joint Surg. Am.*, 70(3):369–376, March 1988.

[4] G E Friedlaender, D M Strong, and K W Sell. Studies on the antigenicity of bone. I. Freeze-dried and deep-frozen bone allografts in rabbits. *J. Bone Joint Surg. Am.*, 58(6):854–858, September 1976.

[5] A Krogh. The number and distribution of capillaries in muscles with calculations of the oxygen pressure head necessary for supplying the tissue. *J. Physiol.*, 52(6):409–415, May 1919.

[6] J E Fletcher. Mathematical modeling of the microcirculation. *Math. Biosci.*, 38(3-4):159–202, April 1978.

[7] A.S. Popel. Theory of oxygen transport to tissue. *Crit. Rev. Biomed.*, 17:257–321, 1989.

[8] J E Fletcher. On facilitated oxygen diffusion in muscle tissues. *Biophys. J.*, 29(3):437–458, March 1980.

[9] J E Fletcher and R W Schubert. Axial diffusion and wall permeability effects in perfused capillary-tissue structures. *Biosystems*, 20(2):153–174, 1987.

[10] N S Abdullah and D B Das. Modelling nutrient transport in hollow fibre membrane bioreactor for growing bone tissue with consideration of multi-component interactions. *Chem. Eng. Sci.*, 62(21):5821–5839, November 2007.

[11] G S Beavers and D D Joseph. Boundary conditions at a naturally permeable wall. *J. Fluid. Mech.*, 30(1):197–207, 1967.

[12] N S Abdullah, D B Das, H Ye, and Z F Cui. 3D bone tissue growth in hollow fibre membrane bioreactor : implications of various process parameters on tissue nutrition. *Int. J. Artif. Organs*, 29(9):841–851, 2006.

[13] N S Mosier, C M Ladisch, and M R Ladisch. Characterization of acid catalytic domains for cellulose hydrolysis and glucose degradation. *Biotech. Bioeng.*, 79(6):610–618, 2002.

[14] B D Wood, M Quintard, and S Whitaker. Calculation of effective diffusivities for biofilms and tissues. *Biotech. Bioeng.*, 77(5):283–598, 2002.

[15] O Bagdasar, C Bailey, R Carter, C Catt, L Dyson, R Dyson, L Geris, G Jones, K Landman, J Malda, J Moles, C Please, S Reboux, Z Rong, T Roose, B Sengers, and M Shakeel. Implants for osteochondral repair using cell printing. In *7th UK Mathematics in Medicine Study Group*, Southampton, 2007.

[16] N S Abdullah, D B Das, and D R Jones. Modelling nutrient transport in hollow fiber membrane bioreactor with consideration of sub cellular scale mass transfer. In *Proc. COMSOL Users Conf.*, Grenoble, 2007.

[17] C Bailey, R Booth, S Cartmell, L Cummings, R Dyson, V Michael, S Naire, L Parsons Chini, S Payvandi, Z Rong, S Waters, R J Whittaker, and H Woollard. Optimisation of fluid distribution inside a porous construct. In *6th UK Mathematics in Medicine Study Group*, Nottingham, 2006.